



Study on the grinding behavior of laser-structured grinding in silicon nitride ceramic

X. H. Zhang^{1,2} · D. D. Wen¹ · Z. H. Deng³ · S. Li¹ · Q. P. Wu^{2,3} · J. Jiang¹

Received: 25 September 2017 / Accepted: 6 February 2018 / Published online: 28 February 2018
© Springer-Verlag London Ltd., part of Springer Nature 2018

Abstract

Silicon nitride ceramics are extremely difficult and time-consuming to be machined with conventional methods, such as turning and grinding. Laser-assisted machining has been a field of extensive research during the past decade, as it is a promising solution to enhance the machinability of many difficult-to-cut materials, including silicon nitride ceramics. To enhance the processing precision of silicon nitride ceramic grinding, in this work, a method of laser structuring the surface of silicon nitride is proposed. The laser process allows to precisely control the dimensions of the generated features. Therefore, different patterns with equal silicon nitride surface area are produced in order to study the influence of the pattern geometry on the grinding behavior of the silicon nitride. Grinding performance of the structured silicon nitride is tested. The influences of grinding parameters, such as wheel speed and feed rate, are analyzed for their effects on the grinding force, surface roughness. It is found that the procedure of laser-structured silicon nitride has a strong influence on the grinding results. The grooves obtained by laser-structured silicon nitride are favorable for the flow of coolant, and the cracks generated inside the grooves weak the material locally. The laser-structured silicon nitride generally allows for a reduction of grinding forces by up to 63%, and it can effectively reduce the wear of the tool.

Keywords Laser structuring · Silicon nitride ceramic · Topography · Grinding force · Surface roughness · Wheel wear

1 Introduction

Difficult-to-cut materials, such as ceramics and titanium alloys, are widely used in various industries because of their good mechanical properties. It is known that silicon nitride ceramic is an excellent high-temperature resistance material which has outstanding physical properties, such as high elastic modulus, low density, and low coefficient of friction [1]. Regarding these properties, silicon nitride has been widely used in aerospace, national defense, and other important industrial areas [2]. Abrasive processes and among them grinding process using diamond grinding

wheels is the most common method for engineering ceramics machining. However, the great hardness and brittleness associated with engineering ceramics cause high grinding forces, low material removal rate, high wheel wear, as well as surface and subsurface damage. Therefore, investigating effective machining techniques for improving the grindability of engineering ceramics has become an active research topic [3–5]. Huang et al. [6] investigated the effect of the grinding wheel speed on the material removal mechanism and ground surface quality. The results showed that the effect of the grinding wheel speed on the ground surface quality was insignificant for a grinding wheel of a large grain size, but the ground surfaces exhibited a predominantly ductile flow and were significantly influenced by the grinding wheel speed when using a wheel with a small grain size. Chen et al. [7] investigated and analyzed the factors that influence the surface quality of brittle materials during ultra-precision grinding. The results showed that the average abrasive grain size of the diamond wheel had the main influence on the surface quality, while the influence of the wheel speed and feed rate were secondary. Li et al. [8] carried out studies to determine the material removal rate of Si₃N₄ during single-pass grinding. The results suggested that there was an optimum depth of cut that yielded the greatest material removal rate. If the grinding depth is larger than

✉ X. H. Zhang
jansbomb@126.com

¹ College of Mechanical Engineering, Hunan Institute of Science and Technology, Yueyang 414006, People's Republic of China

² Advanced Manufacturing Technology Research Center, Liverpool John Moores University, Liverpool 999020, UK

³ Hunan Provincial Key Laboratory of High Efficiency and Precision Machining of Difficult-to-cut Material, Intelligent Manufacturing Institute, Hunan University of Science and Technology, Xiangtan 411201, People's Republic of China

this optimum depth of cut, premature dulling of the diamond wheel occurs, and the grinding surface quality of the Si_3N_4 drastically decreases. Agarwal [9] conducted a study for a high removal rate and studied the effects of various parameters on the surface quality of silicon carbide grinding using a diamond grinding wheel. The results indicated that the material removal was primarily due to micro-fracture and grain dislodgement. The parameters of the depth of cut, feed rate, grit size, and grit density were the primary influencing factors that affect the surface integrity. However, grinding wheel topography changes during grinding. The rapid blunting and wear of diamond abrasives on the wheel surface may cause frequent redressing and shorten the service life of the grinding wheel [10]. As a result, the efficiency of the grinding process and the quality of the workpiece are affected negatively. Wheel wear may induce thermal damage such as surface burn, thus reducing the surface quality [11].

Laser-assisted machining (LAM) is one of the new processing technologies, which uses a laser beam for the processing of difficult-to-machine materials [12]. In recent years, LAM has been shown to be a very promising method to decrease the cost, improve the efficiency, and reduce the surface/subsurface defects. LAM offers important advantages over traditional machining such as reduced power per volume of machined part, higher material removal rate, decreased cutting force, reduced chatter, small residual stresses, reduction of tool wear, avoidance of tool breakage, and crack-free machined surface [13, 14]. LAM has been regarded as a potential machining method for a wide range of hard and brittle materials including ceramics such as alumina, silicon carbide, and silicon nitride. The machinability can be improved because the laser beam is used to abate the strength of difficult-to-cut materials [15, 16]. Shen et al. [17] conducted some fundamental investigations on laser-assisted milling of silicon nitride ceramic. The authors examined the workpiece temperature, the surface integrity, and the tool wear. The effects of laser parameters (laser power, preheat time, and laser beam diameter) and milling parameters (feed rate and cutting speed) were investigated. Yang et al. [18] demonstrated the machinability and feasibility of milling silicon nitride ceramics under laser assistance. It was shown that material removal had more plastic characteristics when the temperature was higher. The cutting forces and specific cutting energy decreased as workpiece temperature increased. No brittle damage to the cutting tool was observed, and surface roughness of the machined surface was comparable to that of ground surface. However, edge chipping, a commonly observed phenomenon during the machining of ceramic material, could not be completely avoided when the temperature was above 1400 °C [18]. In traditional

laser-assisted grinding (LAG), the workpiece area is heated directly before the grinding wheel is engaging; thus, the method permits high stock removal rates [19]. However, if the thickness of the heating layer is greater than the grinding depth, thermal cracks may remain in the subsurface which greatly affects the properties of the machined part. Additionally, the characteristics of traditional LAG limit the use of coolant and also cannot fundamentally eliminate surface/subsurface cracks due to heat accumulation.

From the literature review above, it can be seen that many studies regarding the LAM have been performed. However, their technique is different from the weakening mechanism proposed in this paper. The current work is to structure the silicon nitride surface by laser scanning, and six different structuring patterns are designed. Experiments on silicon nitride grinding are carried out by a diamond grinding wheel, and the effects are studied systematically. The influences of grinding parameters such as wheel speed and feed rate are analyzed for their effects on the grinding force and surface roughness.

2 Experimental

2.1 Experimental materials

The materials used for the experiment are gas pressure sintered and made of Si_3N_4 . The Si_3N_4 workpiece has a hardness of 1700 HV, bending strength of 700 MPa, and elasticity modulus of 320 GPa, as presented in Table 1. The specimens have dimensions of 20 mm × 20 mm × 10 mm. Laser structuring and grinding are performed on the 20 mm × 20 mm surface.

2.2 Experimental setup and method

2.2.1 Step 1: laser structuring

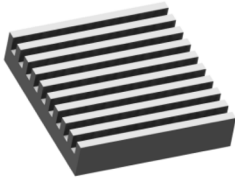
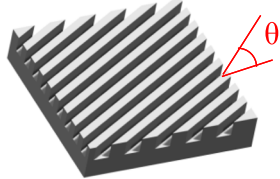
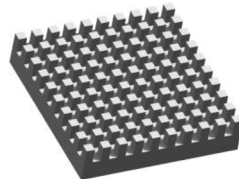
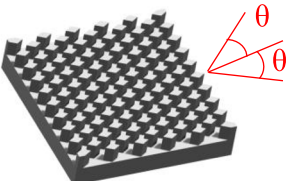
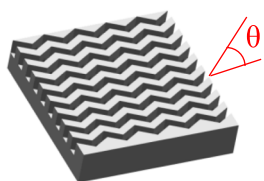
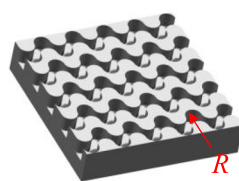
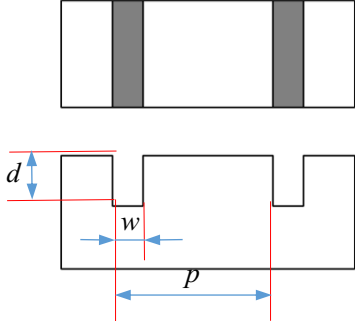
Silicon nitride is structured by using an IPG pulsed fiber laser (model: YCP-1-120-50-50-HC-RG) in the experiment. This laser has an average power (P_{avg}) of 1–50 W, a pulse frequency (f) of 1–200 kHz, a pulse width (τ) of 0.2–25 ms, and a wavelength (λ) of 1064 nm.

In the present work, six different structuring patterns are designed. Table 2 gives an overview of the produced patterns and their dimensions. The characteristic dimensions of the patterns are the groove width w , the groove pitch p , the angular orientation of the grooves θ , the depth of the grooves d , and the radius of the grooves R . In the present study, laser processing parameters are optimized in order to generate a defined groove

Table 1 The properties of the Si_3N_4 workpiece used in the experiment

Density	Hardness	Bending strength	Fracture toughness	Elasticity modulus
3.2 g/cm ³	1700 HV	700 MPa	4.5 MPa m ^{1/2}	320 GPa

Table 2 Overview of the produced patterns and their dimensions

<p>Pattern A:</p>  <p> $d_A = 160\mu\text{m}$ $w_A = 120\mu\text{m}$ $p_A = 320\mu\text{m}$ $\theta_A = 0^\circ$ </p>	<p>Pattern B:</p>  <p> $d_B = 160\mu\text{m}$ $w_B = 120\mu\text{m}$ $p_B = 320\mu\text{m}$ $\theta_B = 30^\circ$ </p>	<p>Pattern C:</p>  <p> $d_C = 160\mu\text{m}$ $w_C = 120\mu\text{m}$ $p_C = 320\mu\text{m}$ $\theta_C = 0^\circ$ </p>
<p>Pattern D:</p>  <p> $d_D = 160\mu\text{m}$ $w_D = 120\mu\text{m}$ $p_D = 320\mu\text{m}$ $\theta_D = 30^\circ$ </p>	<p>Pattern E:</p>  <p> $d_E = 160\mu\text{m}$ $w_E = 120\mu\text{m}$ $p_E = 320\mu\text{m}$ $\theta_E = 30^\circ$ </p>	<p>Pattern F:</p>  <p> $d_F = 160\mu\text{m}$ $w_F = 120\mu\text{m}$ $p_F = 320\mu\text{m}$ $R_F = 250\mu\text{m}$ </p>
		<p> d: structure depth w: structure width p: structure pitch θ: orientation angle R: structure radius </p>

of the desired depth and width in the silicon nitride material, while taking into consideration a minimization of the heat-affected zone. The optimized processing parameters applied to generate the structures are listed in Table 3. The desired groove depth of $d = 160 \mu\text{m}$ is achieved after six repetitions.

Figure 1 shows the three-dimensional schematic of the laser-scanned specimen for the conditions listed in Table 3. The depth of the heat-affected region is 4–8 μm . A thin layer of material (2–5 μm) close to the centerline of the laser scan becomes amorphous and is easily removed mechanically. This is due to the Gaussian nature of the laser beam, which produces temperatures above the dissociation temperature of the ceramic at the center of the laser spot. Materials become gaseous in pulse duration under coupling effect of laser energy and plasma. The ablated surface is covered with silicon and silica only in the course that the material temperature

gradually returned to room temperature. When the temperature of Si_3N_4 goes up due to laser irradiation, thermo-chemical reaction appears to be complicated due to its thermal decomposition and reaction with oxygen. These reactions can be expressed as follows,

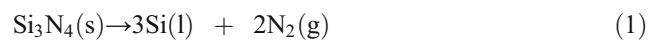
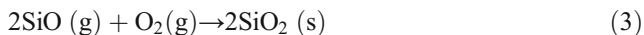
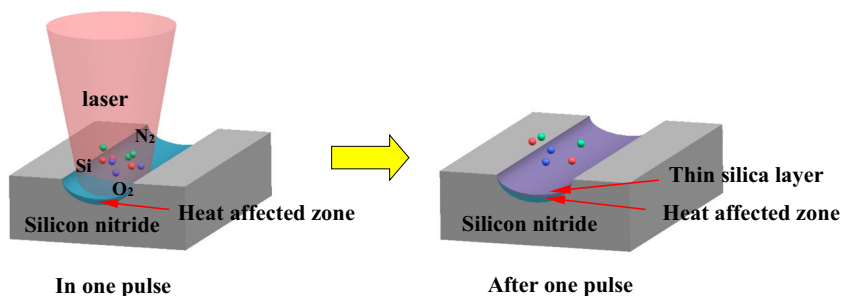


Table 3 The optimized laser structuring parameters

Focal length f [mm]	126
Spot size d_f [mm]	0.06
Average laser power (P_{avg}) [W]	30
Pulse frequency f_p [kHz]	20
Scan speed v_{ss} [mm/s]	2000

Fig. 1 Schematic of laser ablation of Si_3N_4 based on thermo-chemical reaction



2.2.2 Step 2: grinding

Surface grinding experiments are carried out on a CNC high precision surface grinding machine MM9236. The grinding wheel is a diamond grinding wheel typed SDC150N75B. The wheel has a diameter of 200 mm and a width of 20 mm. Before grinding, the grinding wheel is dressed by an electroplated diamond roller dresser (type: S-DC-C-110 \times 12 \times 28) in down dressing mode.

The surface grinding process is a reverse alternating of down-grinding and up-grinding, and the two approaches are similar in grinding mechanism. Thus, one of the processing methods is representative. In the current study, the up-grinding pattern is chosen to investigate the grinding mechanism of the silicon nitride. Various wheel speeds and feed rates are used to study their influences on the grinding performance [20]. Detailed grinding conditions are listed in Table 4. A 3% solution of a soluble water-based Mobil Met 265 HSG Coolant (Mobil Met) is applied to the grinding zone at a flow rate of 25 l/min (with the flow speed of about 1.76 ml/mm² s). Figure 2 shows the schematic diagram of the grinding

Table 4 Grinding conditions

Types	Contents
Machine tool	MM9236
Grinding process	Surface grinding
Abrasive wheels	Resin bond diamond wheel
Grain mesh size	150#
Coolant	25 l/min, emulsion 3%
Wheel speed	50, 90, 120 m/s
Wheel diameter	200 mm
Feed rate	500, 1000, 1500, 2000 mm/min
Depth of cut	50 μm

experiments. The objective is to grind a feature of dimensions 10 mm (L) \times 10 mm (W) \times 180 μm (D). Grinding forces are measured by a dynamometer (model: Kistler 9257A), which is fixed beneath the workpiece and above the worktable of the surface grinder. Transformed by a charge amplifier and a collection card (including A/D converter), the analog signal is amplified and converted into digital signal. Eventually, the grinding signals are stored and displayed on the computer. In addition, the noise signals are filtered by a self-written LabVIEW program, and then the grinding forces of the grinding process are obtained. The roughness of ground samples is measured using a profilometer (model: JB-5C) perpendicular to the grinding direction. In addition, the surface topography is tested by a three-dimensional (3D) microscope with an ultra-large depth-of-field (ULDF) (model: VHX-5000).

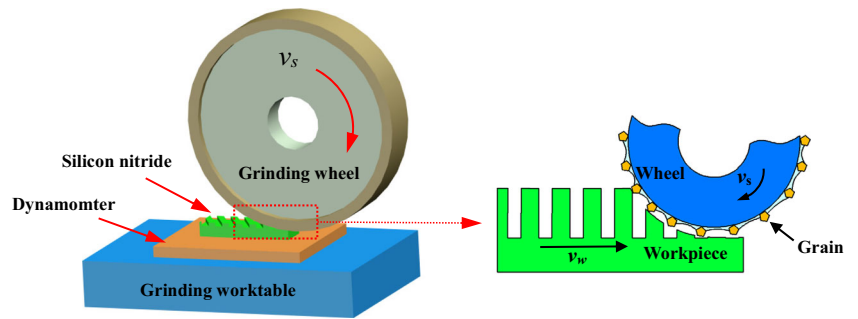
3 Results and discussion

3.1 Silicon nitride surface observation after laser structured

The 3D parameters of the different structured patterns of silicon nitride surface topographies and their local areas corresponding possible thermal deterioration results are presented respectively in Figs. 3, 4, 5, 6, and 7. Figure 3 displays hypsometric topographic maps of the silicon nitride of six different structured patterns. In the figure, blue denotes low-lying areas (i.e., laser-ablated grooves), and red denotes high areas. As the terrain height gradually increases, the graph color gradually changes from blue to red, indicating the undulating terrains of the silicon nitride surface. Figure 4 depicts the 3D topography of the silicon nitride of six different structured patterns.

The internal morphologies of the grooves obtained by laser-structured silicon nitride surface are shown in Figs. 5, 6, and 7. The sidewall of the groove can be divided into two areas. One is the micro-crack area (see Fig. 5c) and the other is a thin and smooth recast layer (see Fig. 5d). The bottom of the groove can be divided into three areas. The first area is the micro-crack area (see Fig. 6d), the second area is the silicon dioxide grain region (see Fig. 6b), and the third area is a rough recast layer (see Fig. 7a).

Fig. 2 Schematic diagram of grinding experimental



The possible reasons for the formation of internal morphologies can be explained as follows. First of all, thermal cracks are produced in the irradiated region due to tensile stresses generated by rapid heating and cooling of the silicon nitride. Then, when Si_3N_4 is machined by laser in air, SiO vapor is formed easily by an oxidation decomposition of Si_3N_4 . Meanwhile, SiO vapor is oxidized immediately and changed to solid phase SiO_2 [21]. A thin molten layer is first formed with the absorption of laser energy. When the molten material reaches the vaporization temperature, the material vapor evaporates from the surface and the melt will be pushed out. As part of this molten material re-solidifies on the sidewall of grooves during the laser machining process, a thin and smooth recast layer is formed. This can also explain the presence of spattering observed outside of the grooves, as shown in Fig. 6c.

When the Si_3N_4 substrate is machined in air, the silicon dioxide grain region is readily formed on the bottom of the grooves. Moreover, there is a noticeable rough recast layer observed in the two overlapping portions of the structured pattern C. This may be because the area of the overlapping portions of the two grooves is relatively high. The condition is disadvantageous to the flow of air. As a result, the material in semi-molten state cannot be carried out by vapor in time and finally re-solidified at the bottom of groove. In addition, the external SiO_2 layer at the wall of the grooves is easy to peel

off. The possible reason is that the thermal stress formed during the laser structuring process contributes to the weak interface adhesion between the re-solidified material and the wall of the grooves [22]. It is worth to note that the formation of the melt will affect the thermal conductivity of the silicon nitride substrates, since SiO_2 has lower thermal conductivity than that of the Si_3N_4 .

3.2 Grinding force

Grinding force is important during the grinding process and has influence on machined surface quality, grinding burning, etc. By range analysis, the variations of the normal force and tangential force with the grinding parameters are shown in Figs. 8 and 9. Force measurements reveal a significant distinction between the different structured patterns. The variations of the grinding forces with the wheel speed in the grinding process are shown in Fig. 8. It can be seen that the normal grinding force is larger than the tangential grinding force in the seven patterns. When the wheel speed is 50 m/s, the grinding force (F_n) in the pattern non-structured is approximately 1.5 times of the pattern D. When the wheel speed is 90 m/s, the grinding force (F_n) in the pattern non-structured is approximately 2.1 times of the pattern D. When grinding the pattern non-structured, the normal grinding force and the tangential

Fig. 3 Hypsometric topographic maps of the silicon nitride of six different structured patterns

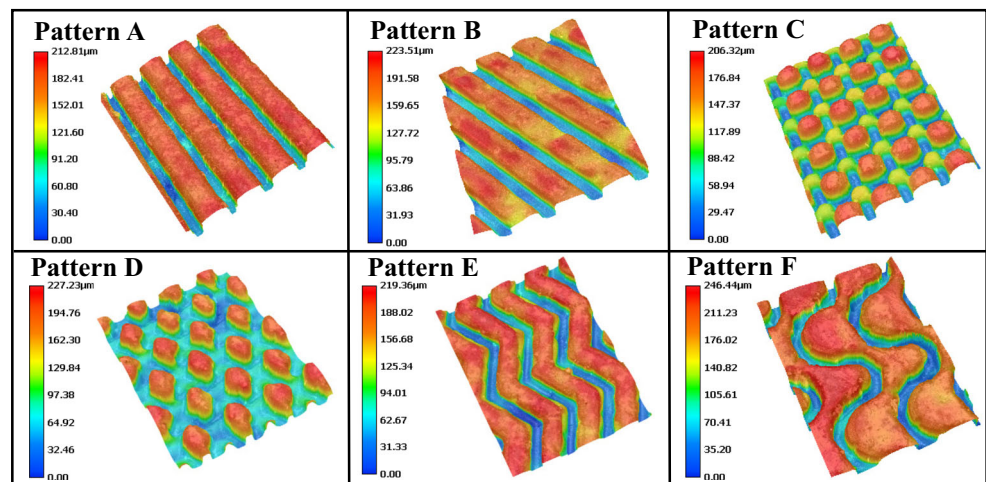


Fig. 4 3D topography of the silicon nitride of six different structured patterns



grinding force are the highest in the seven patterns. In addition, both the normal and the tangential grinding force in different patterns follow this order: non-structured > pattern A > pattern B > pattern F > pattern E > pattern C > pattern D. Furthermore, the figure shows that as the wheel speed increases from 50 to 120 m/s, both the normal and the tangential grinding force decrease obviously.

In essence, the process of grinding structured silicon nitride with diamond grinding wheel is a comprehensive action of the abrasive grains on the workpiece. The analysis of grinding depth of the single grit is conducive to the evaluation of

grinding force. There are many factors that affect the grinding depth of the single grit. The following equation is obtained by analyzing a large number of data and theories:

$$h_m = 0.69 \times \left[\frac{\pi d^3 \tan \gamma}{V_{fa}} \left(\frac{V_w}{V_s} \right) \sqrt{\frac{a_{np}}{D}} \right]^{1/3} \quad (5)$$

Where h_m is the maximum undeformed chip thickness, d is the grain size, 2γ is the vertex angle of the grain tip, V_{fa} is the volume fraction of the abrasive grains, V_w is the constant table speed, V_s is the constant peripheral speed of the wheel,

Fig. 5 The micro-topography of the silicon nitride of structured pattern E

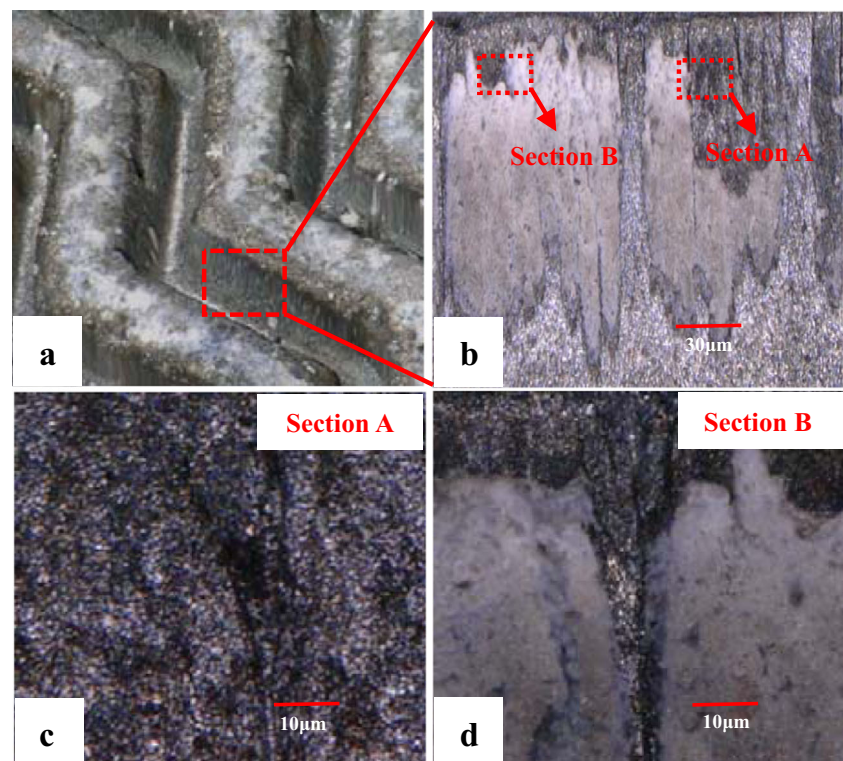
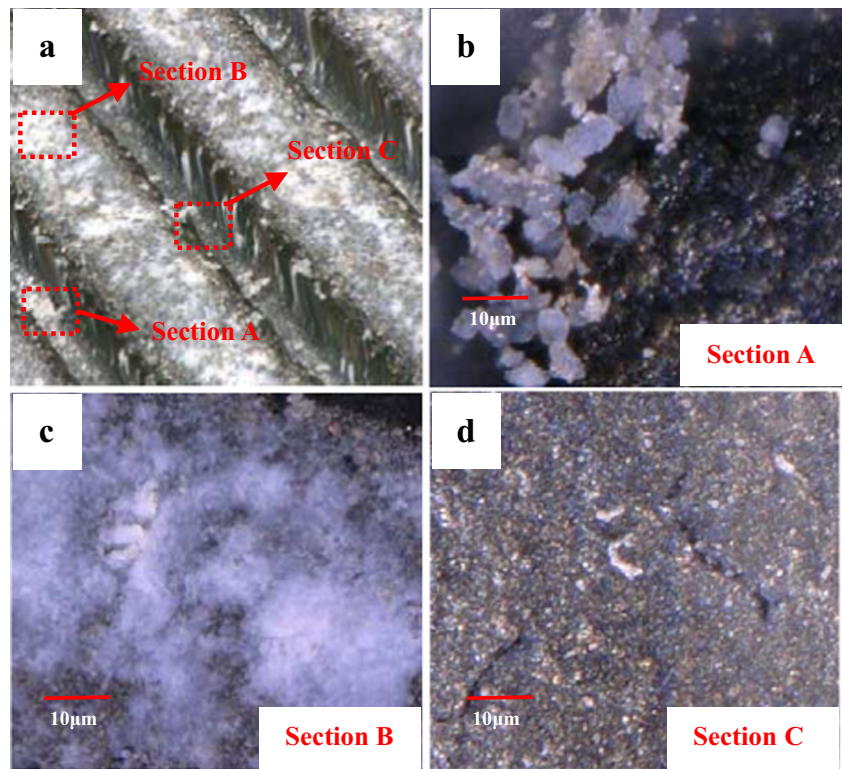


Fig. 6 The micro-topography of the silicon nitride of structured pattern A



a_{np} is the effective wheel depth of cut on the structured pattern, and D is the effective wheel diameter. During the grinding process, the grit travels along a parabolic path, the local chip thickness increases from zero at the origin to the

maximum value. The higher wheel speed leads to a thinner grinding depth of the single grit in the grinding process, which will cause the decrease of the grinding force on the grinding wheel.

Fig. 7 The micro-topography of the silicon nitride of structured pattern C

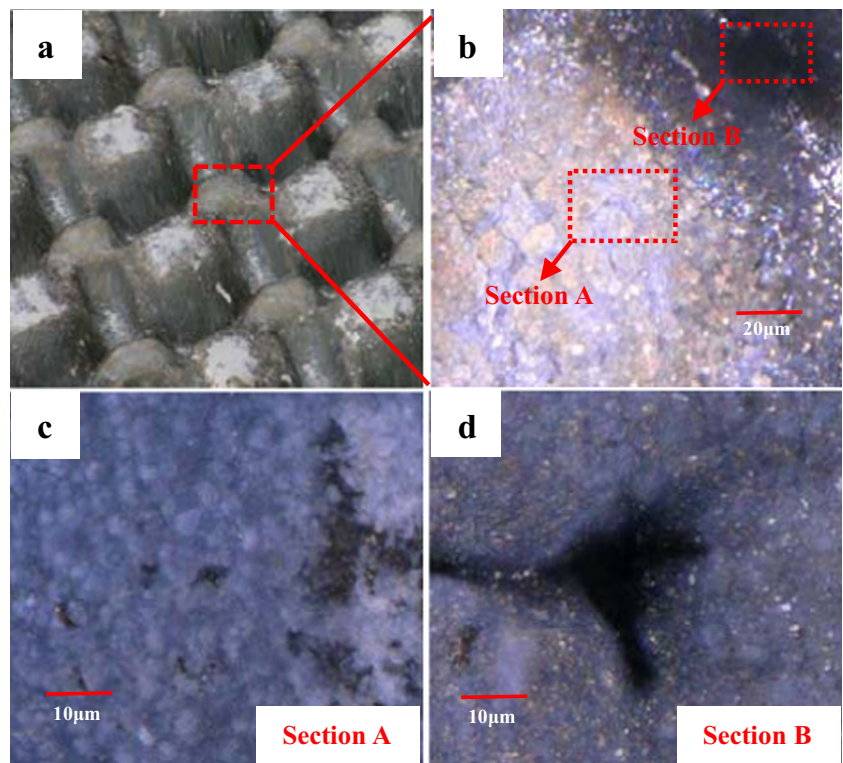


Fig. 8 The effect of wheel speed on the normal force and tangential force (feed rate 500 mm/min). **a** The effect of wheel speed on the normal force. **b** The effect of wheel speed on the tangential force

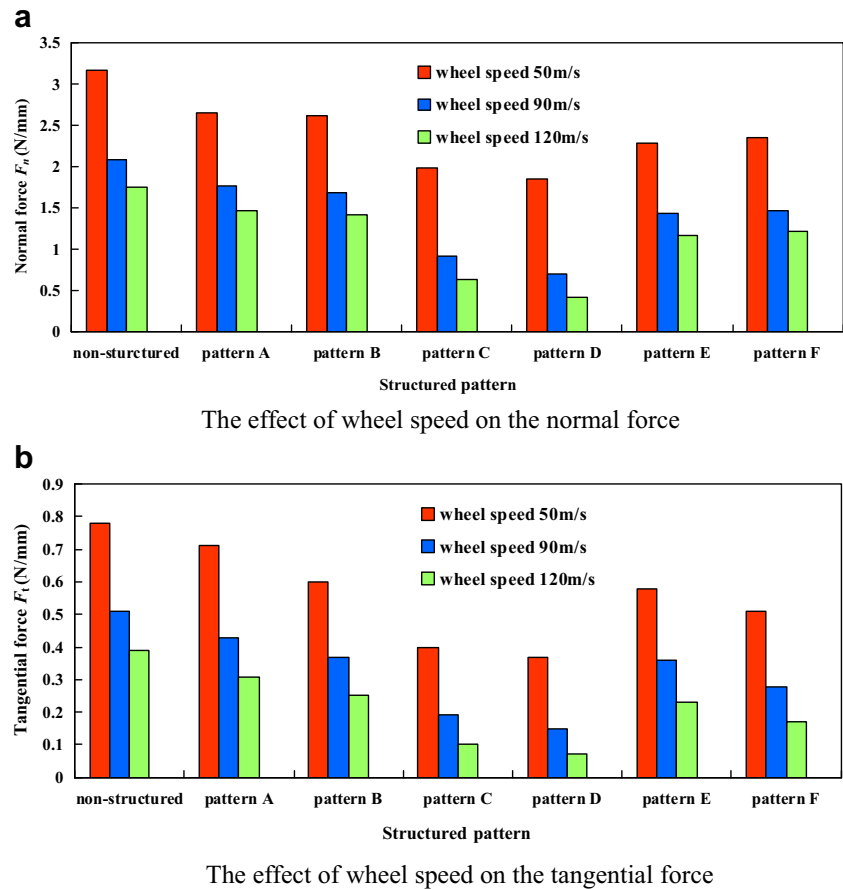


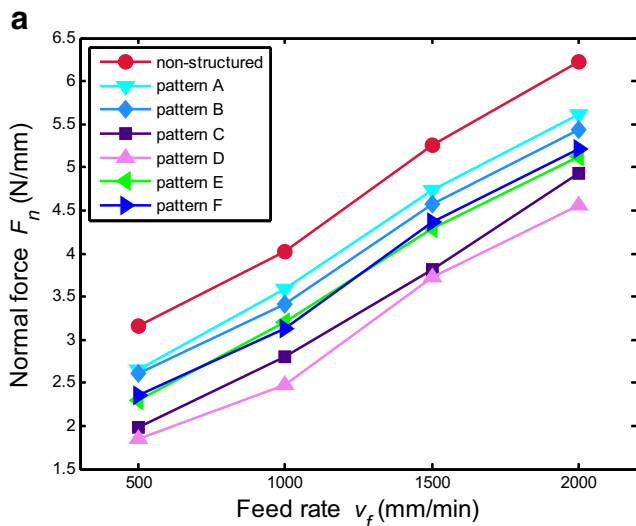
Figure 9 shows the variations of the grinding forces with the feed rate during the test. From the diagram, it can be seen that the non-structured silicon nitride shows the highest force under all tested conditions. The lowest force is achieved by the silicon nitride with surface pattern D. Its force drops by 41% compared to the pattern non-structured. Pattern E and F show a similar behavior with a force reduction between 27 and 25%, while pattern A and B decrease by only 16 and 17%. Therefore, both the normal and the tangential grinding force in the different structured patterns follow this order: pattern non-structured > pattern A > pattern B > pattern F > pattern E > pattern C > pattern D. Furthermore, the figure shows that both the normal and tangential grinding force increase with the increasing feed rate, which is corresponding to the result of Azarhoushang et al. [23]. From Eq. (5), an increase in the feed rate results in a larger undeformed chip thickness and, thus, a larger grinding force.

3.3 Surface roughness

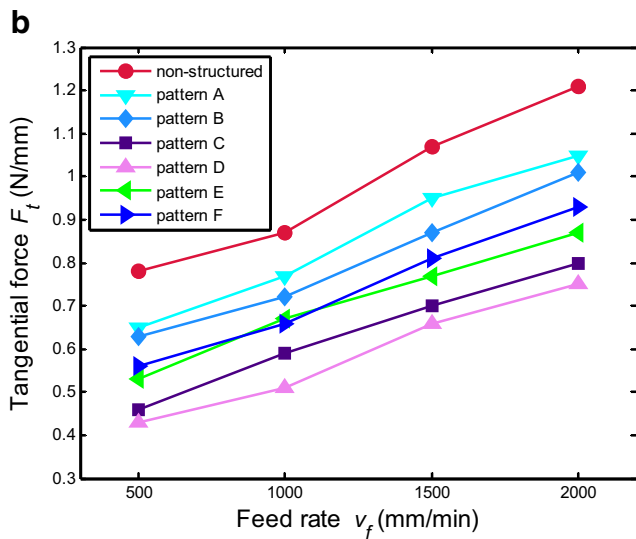
Figure 10 shows the surface roughness of the silicon nitride ceramic grinding in the seven patterns. When the wheel speed

is 50 m/s, the surface roughness R_a in the pattern non-structured amount to $0.38 \mu\text{m}$, compared to the pattern D $0.25 \mu\text{m}$. When the wheel speed is 90 m/s, the surface roughness R_a in the pattern non-structured amount to $0.37 \mu\text{m}$, compared to the pattern D $0.23 \mu\text{m}$. When the wheel speed is 120 m/s, the surface roughness R_a in the pattern non-structured amount to $0.36 \mu\text{m}$, compared to the pattern D $0.21 \mu\text{m}$. When grinding the pattern A, the surface roughness R_a is the highest among the seven patterns. In addition, the surface roughness R_a in various patterns follow the order: pattern A > pattern non-structured > pattern B > pattern F > pattern E > pattern C > pattern D. Furthermore, the figure shows that when the wheel speed increases from 50 to 120 m/s, the increasing wheel speed will cause the decrease of a single grain's undeformed chip thickness, and the surface roughness R_a decreases to some extent. Moreover, the surface roughness R_a decreases obviously in the structured patterns compared to the non-structured pattern.

Figure 11 shows the influence of feed rate on surface roughness R_a . The results indicate that the surface roughness increases with the increasing feed rate. The reason is that the increased feed rate leads to the increasing of the undeformed



The effect of feed rate on the normal force



The effect of feed rate on the tangential force

Fig. 9 The effect of feed rate on the normal force and tangential force (wheel speed 50 m/s). **a** The effect of feed rate on the normal force. **b** The effect of feed rate on the tangential force

chip thickness. When the feed rate is 500 mm/min, it can be noted that the pattern A shows the highest R_a under all tested

Fig. 10 The effect of wheel speed on the surface roughness (feed rate 500 mm/min)

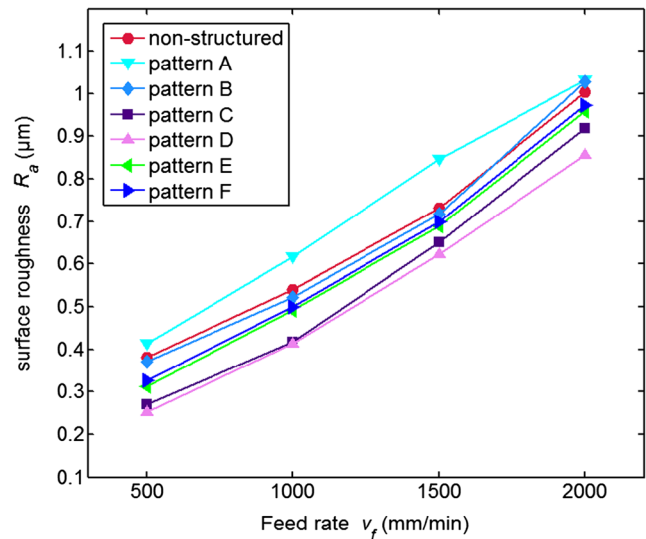
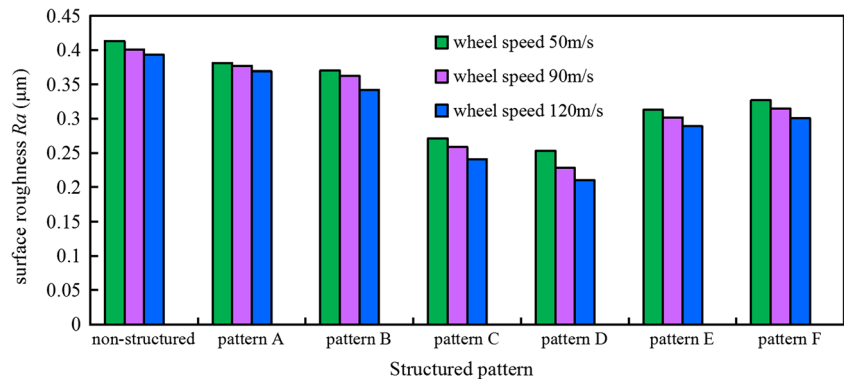


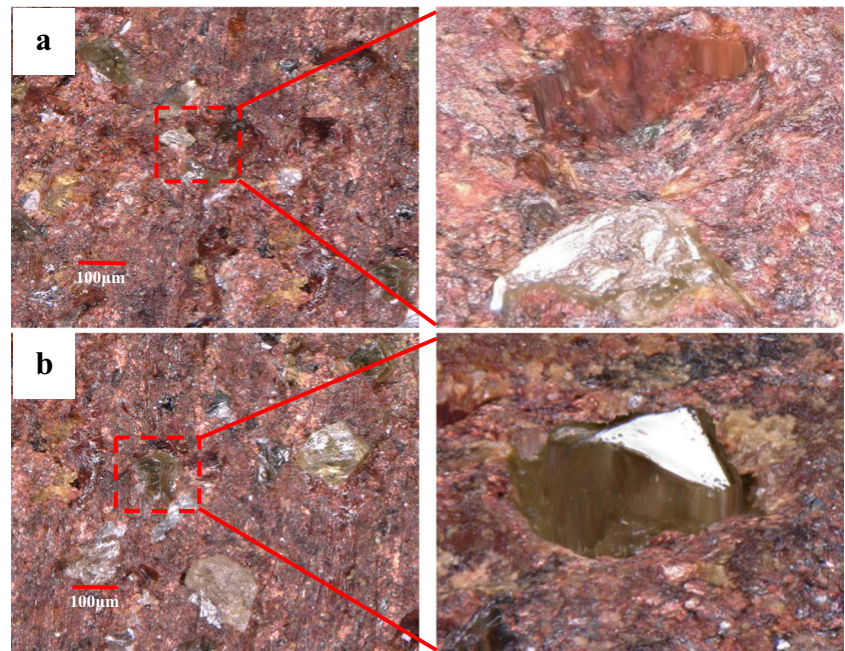
Fig. 11 The effect of feed rate on the surface roughness (wheel speed 50 m/s)

conditions, which R_a raises by 8% compared to the pattern non-structured. The lowest R_a is achieved by the silicon nitride with surface pattern D, and its value drops by 33% compared to the pattern non-structured. Pattern E and F show a similar behavior with a R_a reduction between 16 and 17%, while pattern B decreases by only 3%.

3.4 Wheel wear

Figure 12 shows the surface morphology of diamond wheel after grinding the structured and non-structured silicon nitride, respectively. Figure 12a shows the significant wear of the diamond wheel after grinding the surface of the non-structured silicon nitride. Most of the grits and bonding material on the bottom face of the grinding wheel have been removed. During a grinding process, when the wear of diamond wheel reaches a certain degree, the sharpness of diamond grits will become small. This makes it difficult to sustain a high grinding force for completing this grinding process. As a result, material removal rate will be decreased. Figure 12b shows the surface morphology of diamond wheel after

Fig. 12 The micro-topography of the grinding wheel after grinding the structured and non-structured silicon nitride



grinding the structured silicon nitride. It can be seen that some sharp tips of the diamond abrasives have started to wear. However, the grinding wheel has less wear compared with the wheel grinding the non-structured nitride silicon. This is because when grinding non-structured silicon nitride, the coolant delivery is not very efficient, as the fluid may not adequately penetrate the wheel-workpiece contact zone. But when grinding structured silicon nitride, the grooves contribute to the delivery of coolant. Moreover, the laser-induced cracks on the sidewall of the silicon nitride grooves weaken the material locally, which results in the reduction of the grinding forces and the wear of diamond wheel.

4 Conclusions

In this study, a new laser-assisted grinding method is proposed and applied to produce various micro-patterns on the surface of silicon nitride. Different patterns with equal silicon nitride surface area are produced in order to study the influence of the pattern geometry on the grinding behavior of the silicon nitride. Grinding performance of the structured silicon nitride is tested and compared to a non-structured silicon nitride. The following specific conclusions are derived from this study:

1. The internal micro-topography of the groove obtained by laser-structured silicon nitride surface is measured using a 3D ULDF microscope. The laser-structured silicon nitride yield precise groove depth and satisfactory deterioration effect.
2. The influences of grinding parameters such as wheel speed and feed rate are analyzed for their effects on the

grinding force and surface roughness and compared to the results of a non-structured silicon nitride. The laser-structured silicon nitride generally allows for a reduction of grinding forces by up to 63%, a reduction of surface roughness by up to 35%.

3. The surface morphology of diamond wheel after grinding the structured and non-structured silicon nitride is measured using a 3D ULDF microscope. And laser-structured silicon nitride can effectively reduce the wear of the tool compared to the results of a non-structured silicon nitride.

Future work on laser-structured silicon nitride will examine the effect of the shape of the grooves and optimization of the grinding parameters to obtain even higher material removal rates.

Funding information This project was sponsored by the National Natural Science Foundation of China (grant no. 51405158), the Natural Science Foundation of Hunan Province (grant no. 2016JJ2062), and the Science Research Foundation of Hunan Province Education Department (grant no. 16A089). The authors would thank Dr. Zhongxiong Kang for their experimental support and analysis assistance.

References

1. Kim TW, Lee CM (2015) A study on the development of milling process for silicon nitride using ball end-mill tools by laser-assisted machining. *Int J Adv Manuf Technol* 77(5–8):1205–1211
2. RenJX, KangRK, WangXB (2011) Grinding technology of difficult-to-machine materials. Publishing House of Electronics Industry
3. Zhang B, Fu Y (2013) Grinding of brittle materials with brazed diamond grinding wheel. *Int J AdvManufTechnol* 67(9–12): 2845–2852
4. Shih AJ, McSpadden SB, Morris TO, Grant MB, Yonushonis TM (2000) High speed and high material removal rate grinding of

- ceramics using the vitreous bond CBN wheel. *Mach Sci Technol* 4(1):43–58
5. Chen J, Huang H, Xu X (2009) An experimental study on the grinding of alumina with a monolayer brazed diamond wheel. *Int J Adv Manuf Technol* 41(1–2):16–23
 6. Huang H, Yin L, Zhou L (2003) High speed grinding of silicon nitride with resin bond diamond wheels. *J Mater Process Technol* 141(3):329–336
 7. Chen M, Zhao Q, Dong S, Li D (2005) The critical conditions of brittle-ductile transition and the factors influencing the surface quality of brittle materials in ultra-precision grinding. *J Mater Process Technol* 168(1):75–82
 8. Li W, Wang Y, Fan S, Xu J (2007) Wear of diamond grinding wheels and material removal rate of silicon nitrides under different machining conditions. *Mater Lett* 61(1):54–58
 9. Agarwal S, Rao PV (2008) Experimental investigation of surface/subsurface damage formation and material removal mechanisms in SiC grinding. *Int J Mach Tool Manu* 48(6):698–710
 10. Deng H, Chen GY, Zhou C, Li C, Zhang MJ (2014) Processing parameter optimization for the laser dressing of bronze-bonded diamond wheels. *Appl Surf Sci* 290(3):475–481
 11. Zhang XH, Chen GY, An WK, Deng ZH, Zhou ZX (2014) Experimental investigations of machining characteristics of laser-induced thermal cracking in alumina ceramic wet grinding. *Int J AdvManufTechnol* 72(9–12):1325–1331
 12. Anderson M, Patwa R, Shin YC (2006) Laser-assisted machining of Inconel 718 with an economic analysis. *Int J Mach Tool Manu* 46(14):1879–1891
 13. Kim DH, Lee CM (2015) A study on the laser-assisted ball-end milling of difficult-to-cut materials using a new back-and-forth preheating method. *Int J AdvManufTechnol* 5:1–10
 14. Lei S, Shin YC, Incropera FP (2001) Experimental investigation of thermomechanical characteristics in laser-assisted machining of silicon nitride ceramics. *J Manuf Sci Eng* 123(4):639–646
 15. Navas VG, Arriola I, Gonzalo O, Leunda J (2013) Mechanisms involved in the improvement of Inconel 718 machinability by laser assisted machining (LAM). *Int J Mach Tool Manu* 74(4):19–28
 16. Shen X, Lei S (2011) Experimental study on operating temperature in laser-assisted milling of silicon nitride ceramics. *Int J AdvManufTechnol* 52(1–4):143–154
 17. Shen X, Lei S (2009) Thermal modeling and experimental investigation for laser assisted milling of silicon nitride ceramics. *J Manuf Sci Eng* 131(5):051007
 18. Yang B, Shen X, Lei S (2009) Mechanisms of edge chipping in laser-assisted milling of silicon nitride ceramics. *Int J Mach Tool Manu* 49(3):344–350
 19. Westkämper E (1995) Grinding assisted by Nd:YAG lasers. *CIRP Ann Manuf Technol* 44(1):317–320
 20. Zhao B, Ding WF, Dai JB, Xi XX, Xu JH (2014) A comparison between conventional speed grinding and super-high speed grinding of (TiC_p + TiB_w)/Ti–6Al–4V composites using vitrified CBN wheel. *Int J Adv Manuf Technol* 72(1–4):69–75
 21. Shigematsu I, Kanayama K, Tsuge A, Nakamura M (1998) Analysis of constituents generated with laser machining of Si₃N₄ and SiC. *J Mater Sci Lett* 17(9):737–739
 22. Hanon MM, Akman E, Oztoprak BG, Gunes M, Taha ZA (2012) Experimental and theoretical investigation of the drilling of alumina ceramic using Nd:YAG pulsed laser. *Opt Laser Technol* 44(4):913–922
 23. Tawakoli T, Azarhoushang B (2011) Intermittent grinding of ceramic matrix composites (CMCs) utilizing a developed segmented wheel. *Int J Mach Tool Manu* 51(2):112–119